Large-scale_flowslide_in_Sibalaya_caused_by_the_20181.pdf

by

Submission date: 11-Dec-2021 05:20AM (UTC+0700)
Submission ID: 1727016995
File name: Large-scale_flowslide_in_Sibalaya_caused_by_the_20181.pdf (8.01M)
Word count: 7353
Character count: 37465

Available online at www.sciencedirect.com

ScienceDirect

Soils and Foundations 60 (2020) 1050–1063

www.elsevier.com/locate/sandf

Geo-Disaster Report

Large-scale flowslide in Sibalaya caused by the 2018 Sulawesi earthquake

Mitsu Okamura [a,*], Kohei Ono [a], Ardy Arsyad [b], Utari S. Minaka [a], Sukiman Nurdin [c]

[a] Graduate School of Science and Engineering, Ehime University, Japan
[b] Faculty of Engineering, Hassanudin Unversity, Makassar, South Sulawesi, Indonesia
[c] Faculty of Engineering, Tadulako Unversity, Palu, Central Sulawesi, Indonesia

Received 22 January 2020; received in revised form 15 March 2020; accepted 27 March 2020
Available online 14 August 2020

Abstract

On 28th September 2018, an earthquake of M_w 7.5 hit the Central Sulawesi province in Indonesia. This was followed by liquefaction-induced large-scale ground flows in several areas in Palu city and its neighborhood. A significant characteristic of the ground flows at these sites was that large volume of soil slid downhill along gentle topographic gradients and travelled long distances (more than several hundred meters). To gain a better understanding of the fundamental mechanisms contributing to ground flows, this geo-disaster report summarizes a site investigation conducted at Sibalaya, one of the sites where massive ground flows were observed.

We conducted interviews to reveal the time sequence of the event, including the main shaking that was followed by a sudden drop of the ground surface, the time at which the massive ground flow was initiated (with an extremely loud sound), as well as the change in the water level of wells. Water leakage from the unlined irrigation channel was confirmed to contribute significantly to the increase in the ground water level in this area, which thus increased the liquefaction potential. In situ tests, including eight large trench excavations and dynamic cone penetration tests, were carried out, which helped identify the liquefied and largely sheared layers. An analysis of the change in topography using satellite images and UAV photos also played an important role in capturing the overall picture of the event. Finally, a hypothesized mechanism for the extremely long slide was discussed.

Keywords: Earthquake; Liquefaction; Landslide; In situ test

1. Introduction

An earthquake of M_w 7.5 hit the Central Sulawesi province in Indonesia on 28th September 2018. This was followed by liquefaction-induced, large-scale ground flows in several areas in Palu city and its neighborhood. Four sites with particularly large ground flow incidents were identified: Balaroa, Petobo, Jono Oge, and Sibalaya, located 80–110 km south of the epicenter. An acceleration observatory is located on a bedrock near the Balaroa site, where peak ground accelerations of 203 Gal (NS), 281 Gal (EW) and 335 Gal (UD) were recorded. Detailed information about the earthquake records and the geology of these sites can be found in the papers by Hazarika et al. (2020) and Kiyota et al. (2020).

The massive ground flow areas are situated along the margins of the alluvial flood deposit in the Palu River valley. A significant characteristic of the ground flow at the sites is that ground areas larger than 0.5 km^2 slid downhill along gentle topographic gradients and travelled more than

Peer review under responsibility of The Japanese Geotechnical Society.
* Corresponding author.
E-mail address: okamura@cee.ehime-u.ac.jp (M. Okamura).

https://doi.org/10.1016/j.sandf.2020.03.016

several hundred meters. Such ground flows are a type of lateral spreading, which is a liquefaction-induced deformation phenomenon identified by surficial soil layers breaking into blocks that progressively slide downhill or toward a free face during and after earthquake shaking. Hamada et al. (1986) investigated the horizontal ground displacement of lateral spreading at many sites impacted by the 1964 Niigata and the 1983 Nihonkai-Chubu earthquakes. Bartlett and Youd (1995) and Youd et al. (2002) compiled extensive case histories of liquefaction-induced lateral spreading from many earthquakes mostly in Japan and the U.S. The data ranges were earthquakes with a magnitude of $6 < M_w < 8$ that hit liquefiable sites with a topographical ground slope within the range from 0.1% to 6%. They classified data into two categories: (1) lateral spread toward a free face such as an incised river channel or some other abrupt topographical depression and (2) lateral spread down gentle slopes without a free face. The maximum ground displacement in the case histories was approximately 10 m for the free-face conditions, whereas smaller displacements were observed for the gentle slope conditions. It is obvious that displacements of more than several hundred meters observed at the four sites in Palu are extraordinarily large.

The fundamental mechanism of this unusual event is of particular research interest. We conducted two extensive site investigations: in February and in June 2019. Sibalaya was selected as our target site because the number of houses in the ground flow area was relatively small (approximately a hundred) compared to the other major ground flow areas and no one had been buried alive. By contrast, in other sites, people were believed to be buried alive/missing, making it difficult to conduct site investigations, such as performing excavations or drilling boring holes. Another reason was the ground water condition; unlike other sites, the ground water level in and around Sibalaya lowered after the earthquake, making it easier to excavate trenches for direct visual inspection of the soil profile, including the liquefied layers. Moreover, the Sibalaya site was well preserved and fully accessible during the investigation.

This geo-disaster report summarizes the site investigations conducted at Sibalaya to facilitate a better understanding of the fundamental mechanisms contributing to the ground flows.

2. Interviews of eyewitnesses

Fig. 1(a) presents the location of the Sibalaya site, which is 26 km south of the Palu city center, and whose site topography is an alluvial fan. GEER (2019) adopted the term "flowslide" to describe the massive ground flow after Hungr's classification system (Hungr et al., 2014). This geo-disaster report uses the same term. The flowslide area in Sibalaya shown by the broken line in the figure extended 1100 m from an irrigation canal, upstream to downstream. The solid line indicates the boundaries of the flowslide area before the earthquake and the soil in this area spread, while the boundary translated to the broken line.

A main road passed through the area. There were approximately 60 houses built along this road. Fig. 1(b) shows the locations of the houses where the interviewed residents were living in during the earthquake. A total of 23 residents (ten male and thirteen female), agreed to take part in our survey. All the interviewees felt a strong ground shaking that lasted 10 to 20 s, which is consistent with the acceleration recorded at the observatory near Balaroa. Shortly after the shaking ceased, about several to ten seconds, almost all interviewees felt a sudden drop. This vertical movement after the main shock, was not recorded with the accelerometers near Balaroa, but felt by many people near the flowslide areas on the eastern side of the Palu River, including not only Sibalaya but also the Petobo and Jono Oge areas (Kiyota et al., 2020, GEER, 2019). Then, after about less than a minute, almost all the interviewees heard an extremely loud sound, like structure breaking or thunder. Meanwhile, eight interviewees who stayed close to the flowslide area saw houses and coconut trees moving downslope toward the Palu River at a rate faster than the average walking speed, which lasted about one minute, while soil dust covered the area. Considering the flowslide distance at this site (approximately 350 m), the flowslide speed was likely to be of the order of 20 km/h, which corresponds with that observed in Petobo and Jono Oge (Kiyota et al., 2020). Several interviewees witnessed water from the broken irrigation canal flowing downhill immediately after the movement ceased. All these events occurred within a few minutes. The water continued to flow for almost a day until a canal gate located 8.35 km upstream was closed and the channel dried up.

Information of the ground water level is a key when investigating the liquefaction potential. We found eleven wells at the locations shown in Fig. 1(b) and interviewed their owners. Fig. 2(a) shows a photograph and a schematic illustration of well #1, whose internal diameter and depth were 1 m and 10 m, respectively. Its water level before the earthquake was 5.6 m below the ground surface with small seasonal variations (in the order of a few tens centimeters), which was confirmed through the trace left on the inside wall of the well. Soon after the earthquake, the owner noticed that water overflowed from the well; this overflowing lasted two days. Thereafter, the water level gradually lowered and the well completely dried up in the next two weeks. Although outside the flowslide area, some features typical to areas of liquefaction-induced lateral spreading were detected near the well, including cracks on house walls and fences, house subsidence, as well as sand ejecta on the ground surface. All the other wells, wells #2 - #11, had a similar structure, as shown in Fig. 2(b); a 12-m-long pipe was installed at the bottom of a 4–5.5 m-deep excavated well, through which water was pumped up. They did not observe any water at the bottom of the excavated well before the earthquake, indicating that the ground water level was lower than 5 m in the neighbor-

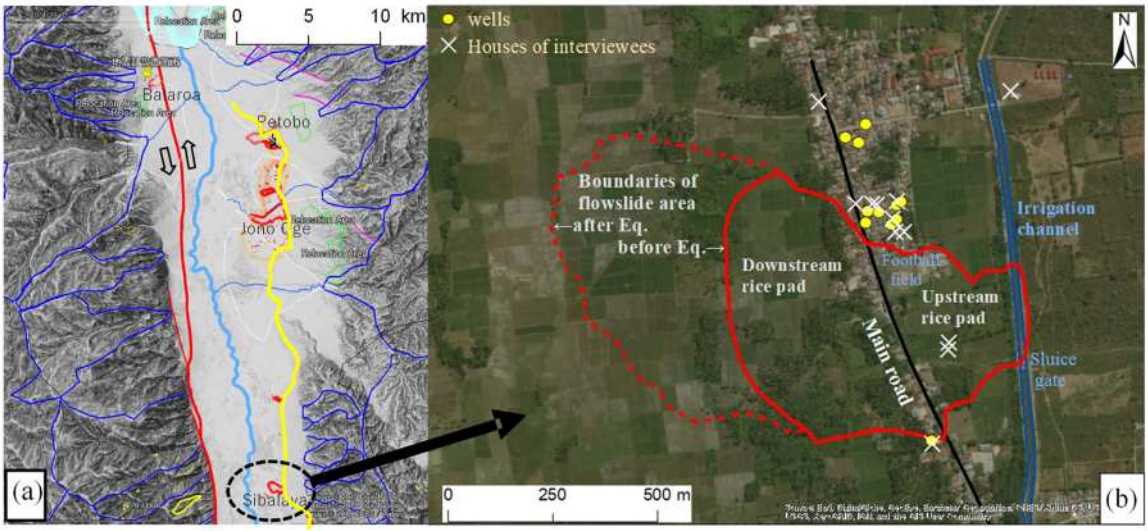

Fig. 1. Locations of major flowslide and houses of interviewed eyewitnesses in Sibalaya. (a) Locations of major flowslide and earthquake fault and irrigation channel (after Kiyota et al., 2020), (b) Satellite image before the earthquake with locations of houses of interviewees, surveyed wells, main road, irrigation channel and flowslide affected area.

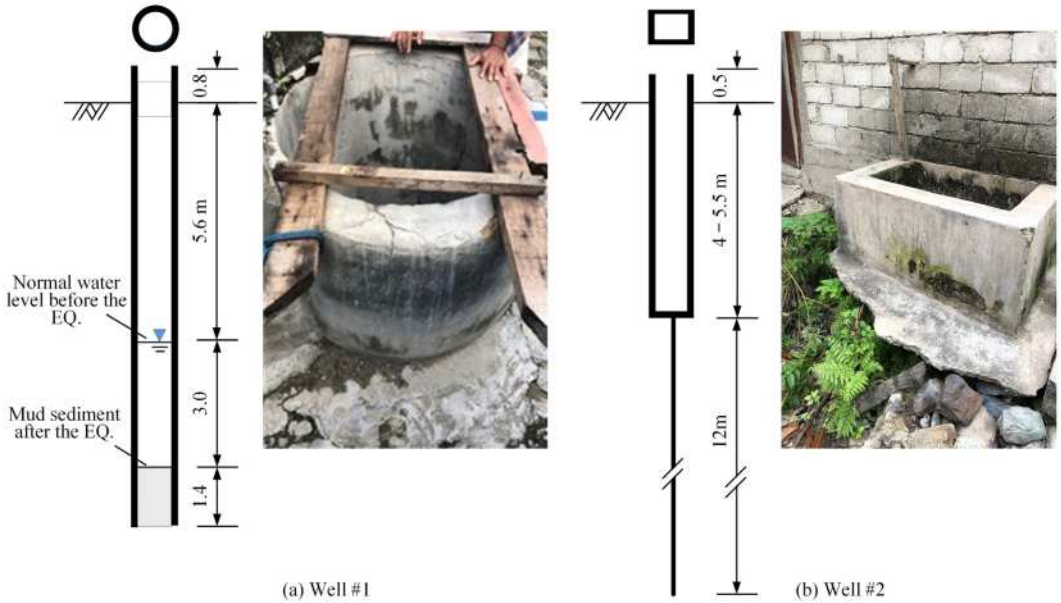

Fig. 2. Photos and cross sections of wells near flowslide area.

hood. Additionally, even several weeks after the earthquake, water could not be pumped up from all the wells except for well #3, whose pipe tip depth was 17.5 m below the ground surface, while for the rest, it ranged between 12 m and 17.5 m. Therefore, it is reasonable to assume that the ground water table was at 5.6 m and 17.5 m before and after the earthquake, respectively.

When it was constructed in the 1930s by the Dutch colonial government, the Gumbasa irrigation channel was a simple dike, and water was used for daily life instead of irrigation. To develop farmland in the neighborhood, the construction works of the Gumbasa irrigation channel began in 1970 and was completed in the 1980s. Since then, the channel has been supplying water for more than 30 years

to rice paddies. It is most likely that water leakage from the unlined irrigation channel allowed water to seep downslope, maintained the ground water level high, approximately at 5.6 m high before the earthquake, which resulted in an increased liquefaction potential.

3. Ground movements

Two orthophotomaps, the World Imagery Map provided by Esri (Esri, 2019) before the earthquake and an assembled map from overlapping UAV photographs obtained using a motion structure software after the earthquake, were used to analyze the ground movements. A total of 25 markers were set in the area to be reflected in photos, whose relative height and locations were surveyed to ensure the accuracy, while the displacement estimation has an accuracy within plus or minus 1 m.

Fig. 3 shows the orthophotomap after the earthquake and photos of several locations. The easternmost margin of the affected area is bounded by the irrigation channel. Arrows in Fig. 3(a) indicate locations and orientations of photos shown in Fig. 3(b)–(j). Concreate panels were

Fig. 3. (a) Orthophotomaps after the EQ (Courtesy by JICA, November 4, 2018). (b)-(j) Photos at locations in and around the flowslide area.

placed on the eastern side surface of the channel, while soil was exposed unlined on the bottom and western sides (Fig. 3(b)). In one southern breached channel section, a box culvert and a sluice gate were heavily damaged, which was most probably the cause of the extremely loud sound heard by the residents. Fig. 3(c) demonstrates the overview of inundation area. There were two major flow paths from the channel that created a cliff as high as several meters (Fig. 3(d)). In this area, as shown in Fig. 3(e), three large blocks were identified, with dimensions of the largest block as 80-m-long and 42-m-wide, that moved about 50 m downwards, which most possibly triggered the irrigation channel failure. Meanwhile, head scarps were formed along the western side of the channel (Fig. 3(f)).

Structures including roads, houses, fences, channel, trees, and footpaths between rice fields were mapped on the two orthophotomaps before and after the earthquake to obtain pre- and post-earthquake locations. Corresponding points were connected to identify the direction and magnitude of ground displacement. The derived displacement vectors are presented in Fig. 4 together with topographic contours before the earthquake at 1-m intervals. Note that the number of mapped points added up to 280; all the points were used to evaluate the strain distribution in the area as described later in Fig. 5. However, in Fig. 4, only about half of them are presented to avoid unfavorable complication. The flowslide generally moved west-northwest, which was normal to the topographic contours. The largest flowslide displacement was in the northern half of the area, ranging between 320 m and 410 m (average 350 m), while smaller in the southern half. Fig. 3(g) illustrates the original main road pavement remained almost intact even after sliding down 360 m. The displacement decreased near the northern and southern margins of the flowslide area, which distorted the ground and ruined structures. Fig. 3(h) presents the main road pavement torn into pieces near the northern margin. The westernmost margin of the flowslide mass after the earthquake was clearly observed as a terrace 1–2 m higher than adjacent unaffected area (Fig. 3(i)).

The red solid line was drawn to inclusively cover all the vector origins in Fig. 4, representing a boundary before the earthquake between flowslide ground mass and ground that did not flow. The boundary moved west-northwest to the broken line. It is most likely that the ground between the two lines did not move significantly, and soil in the upstream side slid and covered the surface.

Fig. 5 presents a normal strain contours in the east–west direction that provides a clear view of the overall deformation characteristic. Strain is negative (tension) and extremely large in an originally narrow area between the irrigation channel and the large blocks translated downslope. Similarly, in the area of the upstream rice pads that immediately in the downslope side of the blocks (see Fig. 1(b)), large tensile strain ranging between 20% and 60% can be observed. In this area, all the structures, rice pads and trees that had been there were translated about 350 m and failed to survive the earthquake. By contrast, in the area between the upstream and downstream rice pads including the original road, the tensile strain is relatively smaller than surrounding areas or even positive (compression). Meanwhile, in the downstream rice pad area, large tensile strain is observed, which is also confirmed by surficial observation that many crack openings were filled with sand ejecta, with orientations mostly normal to the flowslide direction appeared (Fig. 5(b)). These observations suggest that tensile deformation in the flowslide direction generally prevailed in the flowslide area. However, the area of some 100 m width along with the original main road kept its integrity even after the deformation (Fig. 3(g)), while flowslide displacement of the area was somewhat smaller than the surrounding area. This might be because houses in this area pumped up ground water, which increased in thickness of the unsaturated stiff surface.

In areas outside the flowslide, there also exist clear signs of liquefaction-induced lateral spreading. Fig. 3(j) shows concreate wall cracks with a 15 cm-opening, while the house behind tilted about two degrees, which are typical structural damage commonly presented in areas of liquefaction-induced lateral spreading in past earthquakes. Such evidential incidents were observed in many locations including all those surveyed wells shown in Fig. 2(a), indicating that foundation soil of wider area in Sibalaya indeed liquefied. Similar observations were reported for Petobo and Jono Oge (GEER, 2019; Kiyota et al., 2020; Hazarika et al., 2020). On the other hand, on the east of the irrigation channel, any noticeable indication of soil liquefaction was not found in the field survey and UAV photos, indicating that the irrigation channel affected the liquefaction occurrence. Meanwhile, based on the report by GEER (2019), the irrigation channel provided water for agricultural activities and was unlined until it reached the northern edge of the Petobo slide. The unlined channel allowed water to infiltrate downhill towards the river, which contributed to a higher groundwater table and deposit saturations, while increasing liquefaction potential during earthquake shaking.

In this study, AW3D digital elevation maps with a 0.5 m resolution were used to analyze the pre- and post-earthquake topography of the area, which was developed by the Remote Sensing Technology Center of Japan (2019), and the maps were constructed using satellite imageries acquired by Geo-Eye-1 and WorldView-1, -2, -3 and -4 (Remote Sensing Technology Center of Japan). A sufficient number of good quality imageries are important to obtain a high accuracy map. After several trials, 33 imageries taken from October 2010 to May 2018, were used to construct the map before while nine imageries from October 2018 to July 2019 to map after the earthquake. Fig. 6 (a)–(c) depict elevation and change in height along the flowslide main stream (section A-A'), which was almost perpendicular to most contours. In all figures of Fig. 6, locations of the irrigation channel are set at d = 1340 m. The slope angle shown in Fig. 6(b) before the earthquake

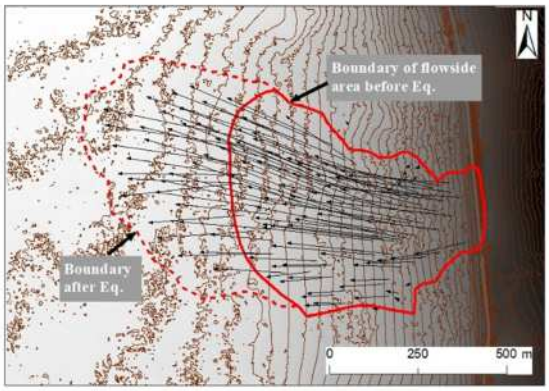

Fig. 4. Displacement vectors and contours before the earthquake.

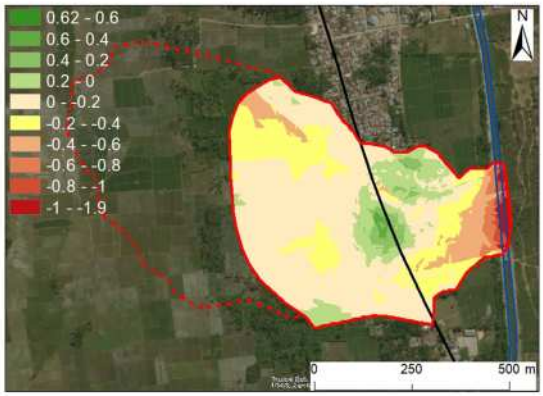

(a) Normal strain in east-west direction ε_x

(b) Many significant cracks appeared in downslope area of the flowslide

Fig. 5. Contours of strain in east–west direction and aerial photo of downslope area.

was three degrees at around the irrigation channel and gradually decreased as going down the slope to approximately zero near the westernmost margin, d = 300 m, where the flowslide finally reached. After the earthquake, the slope was particularly large at around d = 1250 m corresponding to the side cliff of the large block created by flooded water erosion and the adjacent soil flowslide. Change in height (subsidence) was large at the upstream side, decreased to zero at d = 800 m, and turned into heaving until the flowslide margin (d = 300 m), as indicated in Fig. 6(c).

Fig. 6(d)–(f) compare vertical sections of the mainstream (A-A') and the sub stream (B-B'), as well as two sections outside the flowslide area (C-C' and D-D'), in which all the sections were chosen to be parallel to each other. The topography of all these sections before the earthquake were quite similar although deformations were significantly different. Differences in conditions other than topography including soil stratification, mechanical properties of soil and ground water table, should be the reasons for the different deformations between the sections.

Fig. 7 represents change in height in the flowslide and surrounding areas. The area of the flowslide represented by the polygon in red in Fig. 4 is 534,700 m^2, consisting of 339,200 m^2 subsiding area and 195,500 m^2 heaving area. The total volume of subsidence and heaving are 609,900 m^3 and 745,900 m^3, respectively. Consequently, the average subsidence over the entire flowslide is 0.25 m, while that of the area outside the flowslide is also estimated to be 0.013 m, with the subsidence in the area in the east of irrigation channel being generally very small.

4. Identification of liquefied layers

To better understand the underlying mechanism of the extraordinary long distance flowslide, the liquefied layer detection is crucial, which most probably has triggered the event. One common geotechnical practice to identify the liquefied layer depth is to conduct penetration test. About one month after the earthquake, JICA (Japan International Cooperation Agency, 2019) excavated a boring hole to conduct standard penetration tests near the original main road. Sand layers contained gravels and had SPT-N values that are generally high enough to be judged non-liquefiable, high-accuracy liquefied layer identification was challenging. In addition to the triggering factor of the liquefaction, the consequence that the extremely large flow distance is another major subject of interest in this study. Liquefied layer might have been highly disturbed and mixed with immediately above and below soil layers during sliding. Therefore, we decided to excavate relatively large trenches in the flowslide area to expose soil layers including liquefied and non-liquefied layers. It was expected that direct observations on the trench walls helped us to identify the liquefied layer and to provide detailed insight into the mechanism of the unprecedented phenomenon. These trenches also allowed us to obtain soil samples from arbitrary layers for laboratory tests.

Totally seven trenches were excavated in the flowslide as indicated in Fig. 8. Tree trenches, #1 to #3, were excavated in the area where ground surface originally existed upstream side before is resting on the underlying original layers after the earthquake. In this area, shallower soil

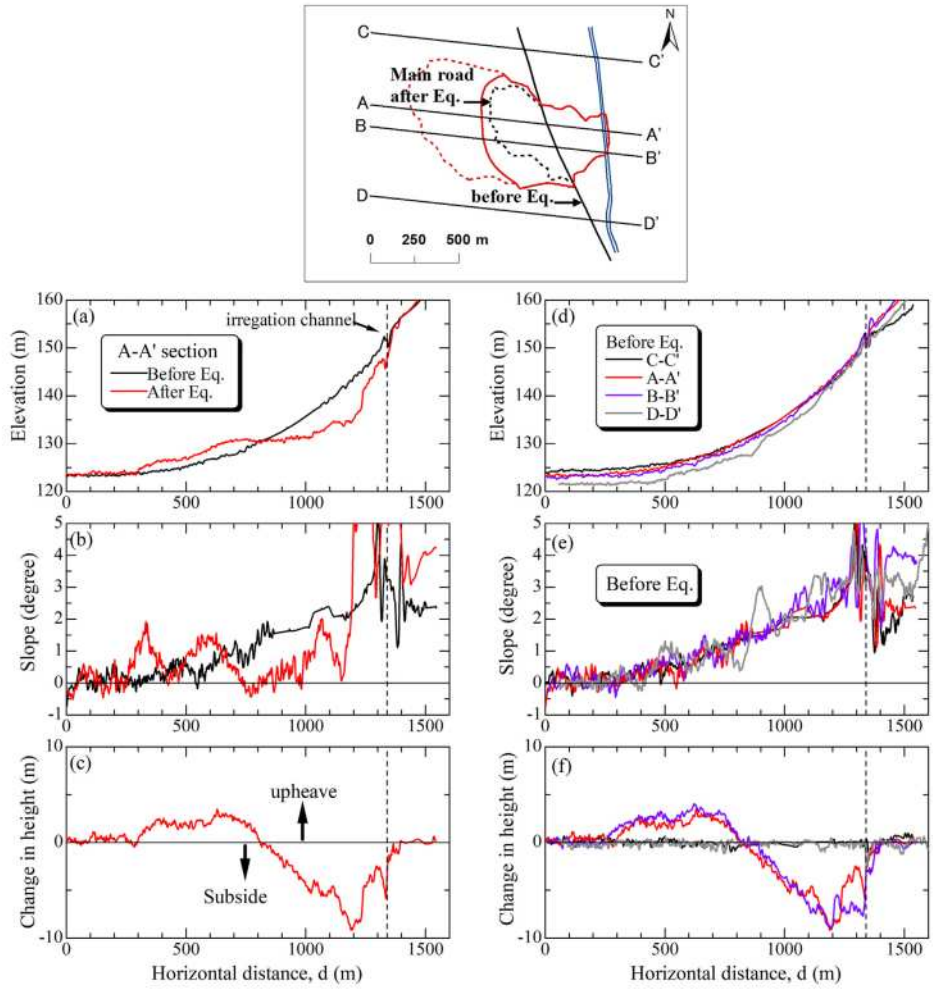

Fig. 6. Height of ground surface in sections parallel to the flowslide.

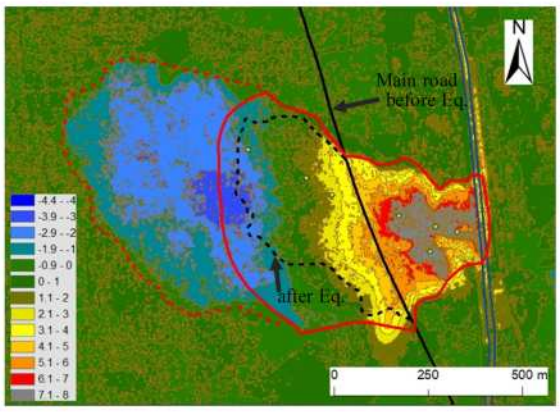

Fig. 7. Contours of change in elevation (in meter).

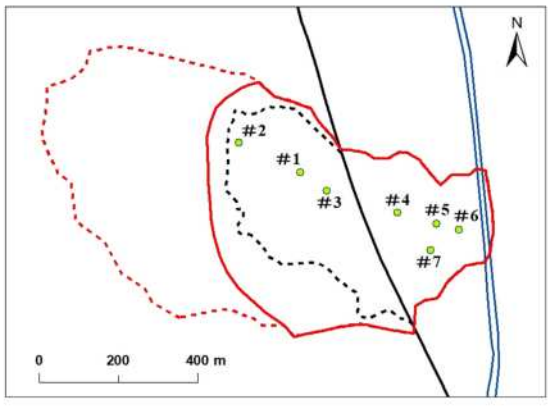

Fig. 8. Locations of excavated trench.

was expected to be highly disturbed and mixed with immediately above and below soil layers. Large trenches, with dimensions approximately being 20-m-long and 5-m-wide, were excavated more than 5 m deep until encountering a non-liquefied layer. While for the trench locations from #4 to #7, where most of the original shallower soil layers had left, eroded by the following flooding and flood sediments deposited on the surface, smaller trenches were excavated until a non-liquefied original soil layer was encountered. The observations of all the trenches are described below, with an exception of trench #7 of which location was apart from the mainstream of flowslide.

4.1. Trench #1

Fig. 9(a) shows an UAV photo of the trench #1, whose ground surface had been in the upstream rice pad, approximately 150 m downslope of the irrigation channel and 200 m upstream of the original main road. A 17-m-long and 5-m-wide area was excavated with the longitudinal axis parallel to the flowslide direction. White lines perpendicular to the flow direction are cracks filled with ejecta from liquefied layers formed by the tensile deformation (See Fig. 7). Meanwhile, smaller cracks parallel to the flow direction are also observed. Fig. 9(b) and (c) present the east and the south walls of the trench, respectively. Considering stability, all the walls of the trenches in this report were cut at a slope angle of 75-degree or less (approximately 1H:3V slope). The east wall cut a crack while there exist ejecta at around the south-east corner. Fig. 9(d) illustrates sketches of the walls. The ground surface was covered with a paddy soil containing stalks and roots of rice overlaying a thin silt layer. These layers were mostly intact, but a difference was noted with respect to the south east corner of the trench. A gravelly sand layer underlying these surface layers was configured by several sand and sandy gravel layers of 10–30 cm thick, with a few thin silty sand layers with thicknesses of the order of ten cm sandwiched in between. The surface of this layer drooping towards the south-east corner suggests that this layer was liquefied and was squeezed near the corner. A thin stiff silty clay layer, which was separating two gravelly sand layers, was found to remain intact except for the corner. The lower gravelly sand layer was mostly uniform with only a few thin interlayers included near to its bottom. It has been observed in all the exposed walls that the typical configuration of non-liquefied gravelly sand layer was a stack of sand and sandy gravel layers every 10–30 cm thick, with thin silty sand layers having thicknesses of the order of ten centimeters sandwiched in between. This fact suggests that both the upper and lower gravelly sand layers liquefied, but due to the flowslide, only the lower gravelly sand layer highly sheared. Stratifications and thin interlayers in this layer were disappeared during long distance flow deformation. The sandy silt layer at the bottom of the trench contained thin interlayers of silt and fine sand (of

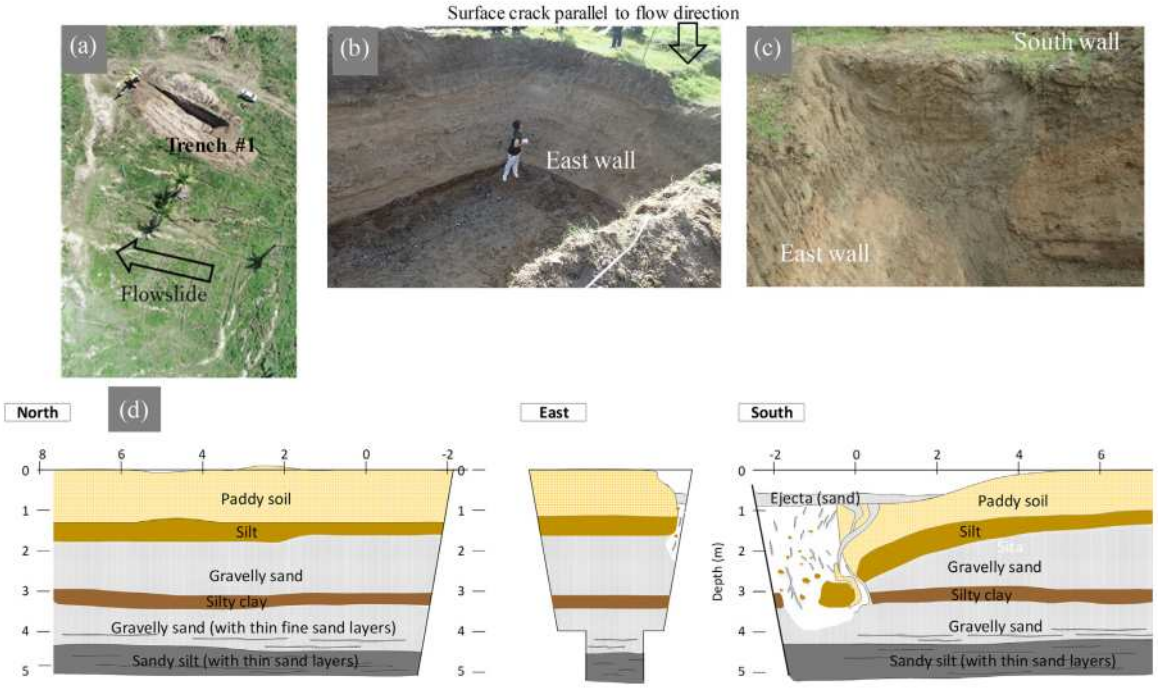

Fig. 9. Trench #1 and its walls. (a) Aerial photo (b) North and west walls in the trench (c) South-east corner in the trench (d) Sketches indicating stratification of soil layer exposed on the walls.

the order of one cm thick) with its surface being level and flat. Furthermore, the soil at the south-east corner is highly disturbed, a part of the silty clay layer was distorted and sand dikes extended from lower sandy gravel layer to the surface while many small fragments of fractured silt layer were contained.

4.2. Trench #3

Fig. 10(a) shows an UAV photo of the trench #3 located at 80 m upstream from the trench #1. The ground surface had been the upstream rice pad, located approximately 70 m downslope of the irrigation channel. This trench had dimensions of 15-m-long and 5-m-wide, with the longitudinal axis parallel to the flowslide direction. Fig. 10(c) presents sketches of the north and the south walls, indicating that the overall figure of the soil stratification is similar to that of trench #1. There were three gravelly sand layers below the surface paddy soil separated by thin silt layers. The gravelly sand layer at the greatest depth was largely uniform and did not have any laminar and interlayers, while the other two gravelly sand layers at shallower depths had. Moreover, the silt and fine sand layer at a depth from 3.5 m and 4 m from the surface seemed intact. Thus, it can be claimed that the liquefied and largely deformed layer is the lower gravelly sand layer.

It should be noted in the north wall sketch that a part of the shallower layers fell into the underlying lower gravelly sand layer, which is a typical deformation pattern that can be observed in the trap-door-experiment (e.g. Stone and Wood, 1992). The soil mass clearly defined by the two conjugate slip surfaces behaved as a block, suggesting that the upper and middle gravelly sand layer did not liquefy. The block located immediately below the white band appeared on the ground surface (Fig. 10(a)), which is described as a tensile crack filled with ejecta.

4.3. Trench #2

Fig. 11(a) illustrates an UAV photo of the trench #2, which was located at 175 m downstream from the trench #1. The surface of the ground had been a soccer field, 20 m upslope from the original main road. This was the largest trench with dimensions of 20-m-long and 5-m-wide while the longitudinal axis approximately normal to the flowslide direction. It can be seen in Fig. 11(b) that a slip line (shear zone) passed through and divided this area into two blocks. Referring a house and a torn-off fence shown

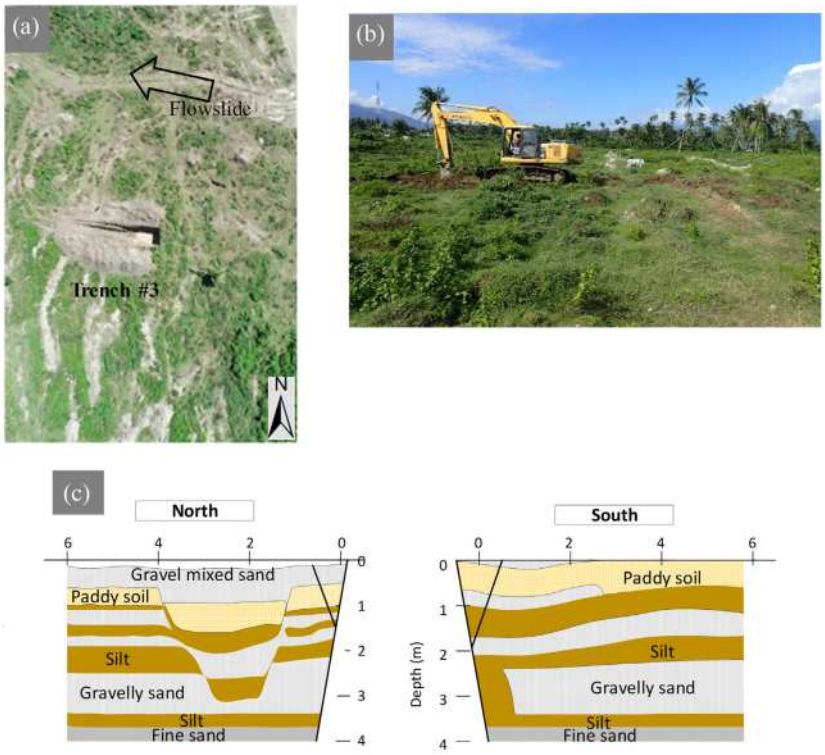

Fig. 10. Trench #3. (a) Aerial photo (b) Site of the trench just before the excavation initiated (c) Sketches indicating stratification of soil layer exposed on the walls.

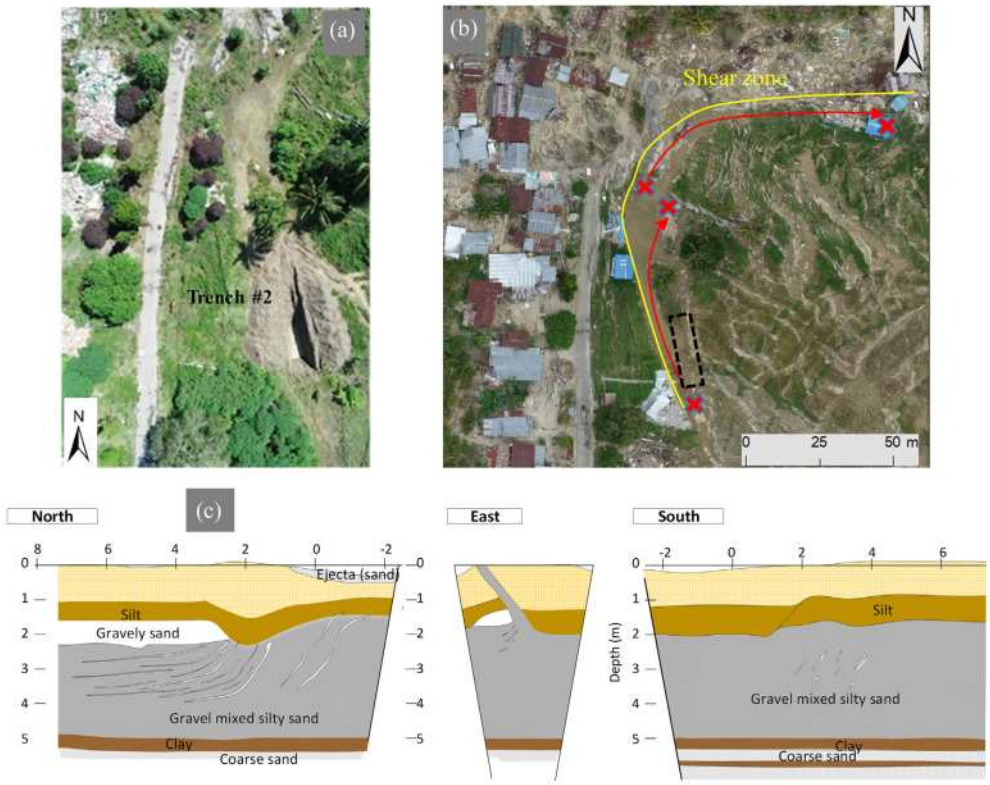

Fig. 11. Trench #2. (a) Aerial photo of the trench #2 (b) Orthophotomap of the wider area around the trench after the earthquake (c) Sketches indicating stratification of soil layer exposed on the walls.

by red crosses in the figure, the movement of the east side block relative to the west side block is estimated to be 55 m. The trench #2 was excavated on the shear zone between the two blocks. Fig. 11(c) demonstrates sketches of the north, east and south walls. A surface layer with silt layer underneath was similar to those in the trenches #1 and #3, while with a difference that a single thick sandy gravel layer was found below the surface layers, which was highly disturbed with apparently higher fines content in contrast to the trenches #1 and #3. Many clay fragments and dikes of clean fine sand with several centimeters width randomly existed, indicating that the layer was highly disturbed. It can be assumed that this layer was consisted of multiple sandy gravel layers, which were separated with thin silt layers but mixed altogether due to the extremely large shear deformation during the flow sliding. Thin interlayers of silt or fine sand remained only in a clay and a coarse sand layers at the bottom of the trench.

4.4. Trench #4

Trenches #4 to #7 were excavated at upstream side in the flowslide and in the inundation flow path. Soil stratifications appeared on the trench walls were much simpler as compared to those in the downstream trenches. Fig. 12 shows a photo and a sketch of trench #4. At the ground surface, clean uniform coarse sand loosely deposited to the depth of 1.7 m. The color and grain size distribution of the sand were different from any layers in the downstream trenches #1, #2 and #3. In this layer, a relatively new plastic bag and garbage were found, indicating that it was a fluvial deposit brought by the flooding water from the irrigation channel. From 1.7 to 3 m below the ground surface, there was a highly disturbed layer without any thin interlayers included, whose soil was gravelly sand with many small clay and silt fragments being heterogeneously mixed, and was most likely liquefied and highly sheared as the overlaying surface layers slid downslope. A silt layer at 3 m deep observed as undisturbed, which contained thin interlayers of fine sand remained (several mm in thick).

4.5. Trench #5

Although trench #5 located only 30 m upstream from #4, the width of the inundation flow path at this location was approximately 2.5 times narrower than that at #4, suggesting that flow rate of the flooding water was considerably higher than #4. Fig. 13 indicates photos and a

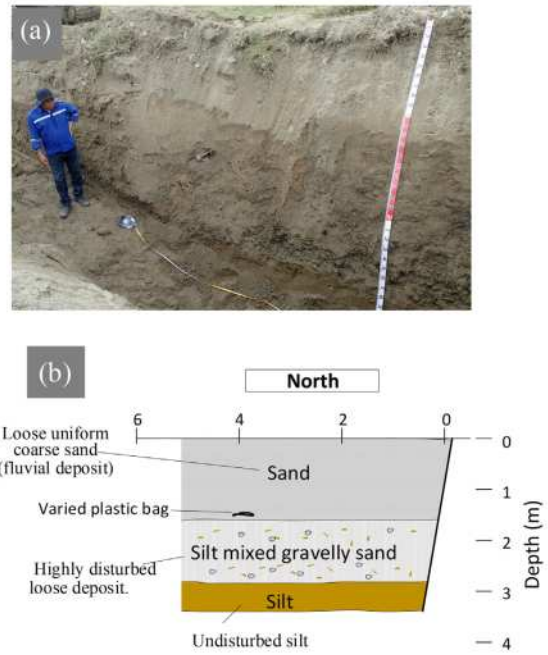

Fig. 12. Photo and sketch of trench #4.

Fig. 13. Photos and sketch of trench #5.

sketch of the trench. The trench was excavated with the longitudinal direction parallel to the flow path. Clean uniform coarse sand, which is considered to be fluvial sand loosely deposited, and an undisturbed silt layer were appeared at a depth of 2 m. A possible scenario of deposit formations at trenches #4 and #5 is that the gravelly sand layers liquefied during the earthquake, while the overlying soils slid down to the slope and liquefied layer been exposed. During the flooding event triggered by the irrigation channel failure, the liquefied gravelly sand was fully flushed by the flooding water at #5, but only the surface of the liquefied sand was eroded at #4 because flooding water spread out and flow rate decreased at #4. Thereafter, the flow rate has slowed down and uniform coarse sand loosely deposited on the surface at both #4 and #5.

4.6. Trench #6

Trench #6 was excavated at 105 m upstream from #5 and 120 m downstream from the irrigation channel on the side of a cliff of one of the large soil blocks and at the flow path edge. Fig. 14 depicts photos of the trench and sketches of the walls. The cliff of the block was 5 m high from the flow path bed and consisted of layers of gravelly sand, silt and silty clay, with all of their thicknesses in a range 10–80 cm. The west wall (Fig. 14(b)) is the cliff of the block. It is reasonable to consider that the gravelly sand layer below the silty clay layer liquefied and sheared, while the overlying soil block slid down approximately 30 m. Soil mass originally existed slid approximately 350 m down to the slope, which highly disturbed the gravelly sand layer in the south and north wall. The fluvial course sand was deposited at the surface while its depth increasing with respect to increase in distance from the cliff.

Ground water was not encountered in all the trenches, which is consistent to the observation that water table in the wells dropped 12 m after the earthquake.

5. Flowslide mechanism

Fig. 15 depicts the cross-section A-A' along with the main stream of the flowslide passing through most trenches excavated in this study, together with depths of identified liquefied layers in each trench. The broken line represents a possible slip surface or a shear zone, along which large

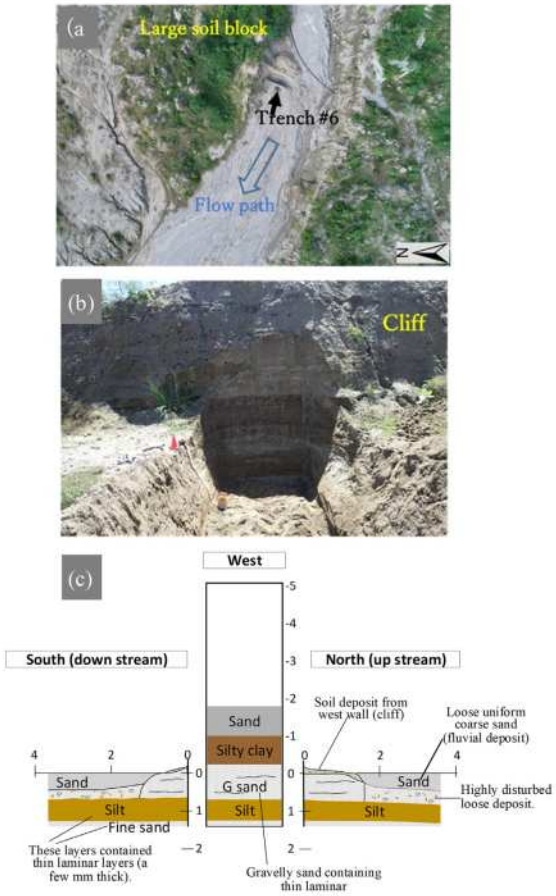

Fig. 14. Photos and sketch of trench #6.

shear deformation is considered to have occurred, and soils above the line slid downslope while that underneath remained.

The flowslide is the consequence of the shear resistance of the zone degrading significantly or being completely lost against the sliding deformation. A soil mass in the flowslide near the westernmost region, which was indicated by the shaded zone in the figure, was chosen as an example. The shear resistance mobilized along the base of the mass, τ_r, can be estimated simply based on the energy conservation as follows:

$$\tau_r = \frac{M_s g}{l \cdot L} \Delta S \approx 2kPa \tag{1}$$

where M_s and l denote the mass and base length of the soil mass, respectively, L is flowslide distance, g is the gravitational acceleration, and ΔS is change in height of the gravity center of the mass. It is noteworthy that the earth thrust acting on the right-hand side boundary of the soil block was regarded as negligible because the boundary height was much smaller than the base length L. Several tensile cracks appeared on the ground surface and tensile strains in this area, as shown in Fig. 5, also supports the premise of Eq. (1), that the thrust was not significant as a driving force. In Eq. (1), energy consumption along with several cracks in the soil mass was neglected for simplicity. The estimated τ_r can be even smaller if the internal energy dissipation along the cracks is considered; thus, the τ_r is the upper bound of the shear resistance. It can be claimed that the shear resistance mobilized on the mass base was 2 kPa or less.

A hypothesis previously presented by Field et al. (1982), Fiegel and Kutter (1994) and Kokusho (1999) to explain the large ground deformation is the formation of water interlayers. In this hypothesis, a water interlayer with practically zero shear strength was formed shortly after shaking immediately above a liquefied layer, which is covered by an overlying less permeable layer. They conducted centrifuge and 1 g shaking table tests to demonstrate the occurrence of delayed ground deformation after shaking, while the soil above the water interlayer slid downslope. This is quite similar to the Sibalaya case in the deformation timing, where the ground started to flow after the earthquake shaking ceased; this was eye-witnessed by multiple residents. In contrast, several potential arguments exist against this hypothesis as follows:

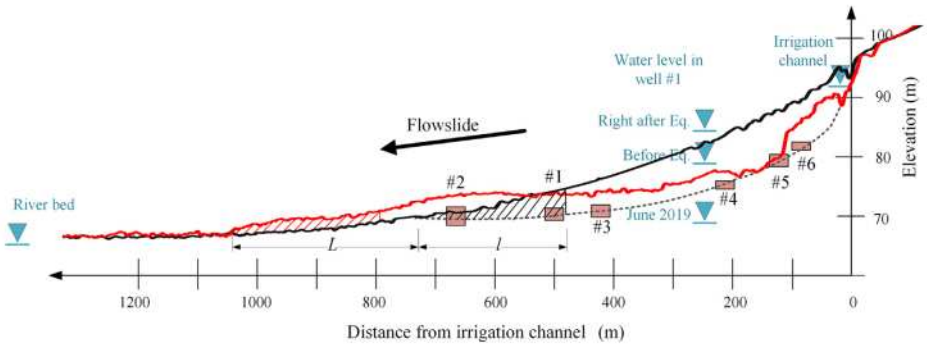

Fig. 15. Cross section of A-A section before and after the earthquake together with highly sheared depths detected in trenches.

- For a soil mass to slide on a water interlayer, the layer should incline even though the shear strength is completely lost in the layer and the ground surface is inclined. The liquefied and highly sheared layer identified in trench #1, #2 and #3 were at almost the same elevation and presumed slip surface, or a water interlayer is practically level.
- The water interlayer should be smooth and continuous over the flowslide area. However, as shown in Fig. 10, the soil blocks dropped into the liquefied layer were present, which made the water interlayer discontinuous and obstructed the soil sliding deformation above the layer as *shear keys*, as illustrated in Fig. 16. The existence of many similar tensile cracks suggested the existence of similar shear key blocks.
- In the trenches it was observed that gravelly sand layers, which were verified to have been liquefied, contained many small silt fragments, while seam layers may have disappeared. This fact suggests that the layers were highly sheared, which could be impossible if shallower layers slid down on the water interlayer without any disturbance of the underlying liquefied layer.

Therefore, the Sibalaya flowslide cannot be fully explained by the hypothesis of the water interlayer alone.

Another possible explanation for the main cause of the flowslide is attributable to the mechanical property of the liquefied soil. If the sand is highly contractive and demonstrated a typical flow type response with a peak strength followed by zero residual strength, an infinitely large strain could be generated. Based on the results of undrained shear tests, Kokusho (2015) claimed that clean sand always exhibits a dilative response and flow-type failure is less likely to occur. However, the presence of low/non-plastic fines mixed with clean sands changes the volume change characteristics significantly. Kokusho conducted undrained monotonic torsional shear tests on loose sand specimens with parametrically increasing non-plastic fines. The soil response changed from dilative to contractive as the fines content increased, and sand with 20% fines exhibited perfect flow with almost zero residual strength. Fig. 17 indicates the grain size distribution of soil obtained from a gravelly sand layer in trench #1, where the sand contained small amount of silt as well as gravel. The fines in the soil was confirmed with laboratory testing to be non-plastic.

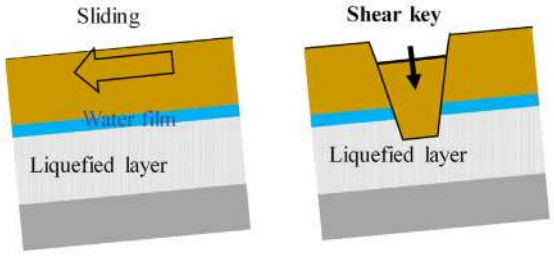

Fig. 16. Schematic illustrations of shear key effects of a part of sliding soil block submerged into an underlying liquefied layer.

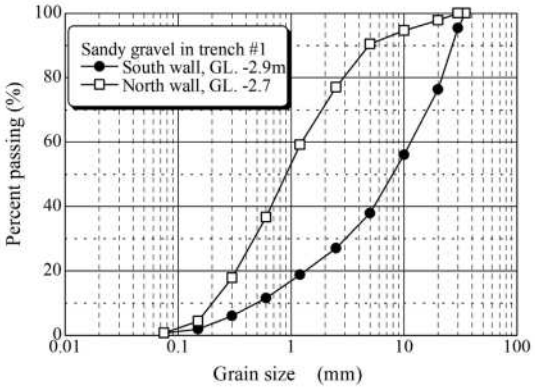

Fig. 17. Grain size distribution of soils obtained from highly sheared layer in trench #1.

6. Summary

In this study, to better understand the fundamental mechanisms, extensive site investigations were conducted at Sibalaya, where an extraordinary long distance flowslide occurred during the 2018 Sulawesi Earthquake. Valuable verbal evidences were collected from many interviewees regarding time sequence of the event. In situ tests including the excavation of eight large trenches were greatly helpful in identifying the liquefied and largely sheared layers. Analysis of topography change using satellite images and UAV photos were also invaluable in obtaining an overview of the event. The following major foundlings were drawn:

- The sequence of events including the main shaking followed by a sudden drop, initiation timing of the massive ground flow and extremely loud sound, flooding, as well as the water level change in a well were confirmed.
- Water leakage from the unlined irrigation channel is regarded to have risen the ground water level in this area, thereby increasing the liquefaction potential.
- Soil in both the inside and outside the flowslide affected area was liquefied, except for that in the area east to the irrigation channel.
- Along with a main stream of the flowslide, tensile deformation prevailed in the ground surface with an exception in the area around the main road.
- Investigating the mechanism of the long distance flowslide is still ongoing. Shear resistance mobilized on the base of flowslide soil mass was roughly estimated to be 2 kPa or less. Although the water interlayer may contributed to some extent, the Sibalaya flowslide cannot be fully explained by the hypothesis of the water interlayer alone.

- Continued large shear deformation of the liquefied sand layer was indicated, which is not a common behavior of sand. This could be possible only if the almost zero-residual strength of the sand was reached and persisted while the sand experienced an extremely large strain. Further study on the mechanical properties of sand in flowslide areas is necessary.

Acknowledgements

The authors would like to express their sincere gratitude to the members of the JICA Domestic Technical Support Committee, in particular, Prof. Kenji Ishihara, Prof. Takaji Kokusho, Prof. Susumu Yasuda, Prof. Ikuo Towhata, Dr. Takashi Kiyota, Prof. Hemanta Hazarika and Dr. Kimio Takeya, for their valuable comments and suggestions. This work was partly supported by the Ehime University President Special Research grant.

References

Bartlett, S.F., Youd, T.L., 1995. Empirical prediction of liquefaction-induced lateral spread. J. Geotech. Eng. ASCE 121 (4), 316–329.

Esri, Inc., 2019. <https://www.arcgis.com/home/item.html?id=10df2279f9684e4a9f6a7f08febac2a9> (accessed 01.10.2019).

Fiegel, G.L., Kutter, B.L., 1994. Liquefaction mechanism for layered soils. J. Geotech. Eng. ASCE 120 (4), 737–755.

Field, M.E., Gardner, J.V., Jennings, A.E., Edwards, B.D., 1982. Earthquake-induced sediment failures on a 0.25° slope, Klamath River delta. California. Geology 10, 542–546.

GEER (Geotechnical Extreme Events Reconnaissance), 2019. The 28 September 2018 M7.5 Palu-Donggala, Indonesia Earthquake, Version 1.0. <http://learningfromearthquakes.org/2018-09-28-palu-indonesia/images/2018_09_28_palu_indonesia/pdfs/GEER_Palu_Version_1.pdf> (accessed 30.09.2019).

JICA, 2019. JICA Domestic Technical Support Committee Meeting

Kiyota, Takashi, Furuichi, Hisashi, Hidayat, Risqi Faris, Tada, Naoto, Nawir, Hasbullah, 2020. Overview of long-distance flow-slide caused by the 2018 Sulawesi earthquake, Indonesia. Soils Found. 60 (3), 722–735 https://linkinghub.elsevier.com/retrieve/pii/S0038080620336209. https://doi.org/10.1016/j.sandf.2020.03.015.

Kokusho, T., 1999. Formation of water film in liquefied sand and its effect on lateral spread. J. Geotech. Geoenviron. Eng. ASCE 125 (10), 817–826.

Kokusho, T., 2015. Liquefaction Research by Laboratory Tests versus In Situ Behavior. In: Proc. 6th International Conference on Earthquake Geotechnical Engineering, Christchurch, New Zealand, pp. 786–819.

Hamada, M., Yasuda, S., Isoyama, R., Emoto, K., 1986. Observation of permanent ground displacements induced by soil liquefaction. Peox. Jpn. Soc. Civ. Eng. 376/III-6, 211–220 (in Japanese).

Hazarika, H., Pasha, S.M.K., Pohit, D., Masyhur, I., Arsyad, A., Nurdin K., 2020. Large distance flowslide at Jono-Oge due to the 2018 Sulawesi Earthquake, Indonesia. Soils and Found. Japanese Geotech. Soc. (Submitted).

Hungr, O., Leroueil, S., Picarelli, L., 2014. The Varnes classification of landslide types, an update. Landslides 11 (2), 167–194.

Remote Sensing Technology center of Japan. https://www.aw3d.jp/en/about/ (accessed 12.08.2019).

Stone, K.J.L., Wood, D.M., 1992. Effects of dilatancy and particle size observed in model tests on sand. Soils Found. Japanese Geotech. Soc. 32 (4), 43–57.

Youd, T.L., Hansen, C.M., Bartlett, S.F., 2002. Revised multilinear regression equations for prediction of lateral spread displacement. J. Geotech. Geoenviron. Eng. ASCE 128 (12), 1007–1017.

Large-scale_flowslide_in_Sibalaya_caused_by_the_20181.pdf

ORIGINALITY REPORT

4%	3%	3%	0%
SIMILARITY INDEX	INTERNET SOURCES	PUBLICATIONS	STUDENT PAPERS

PRIMARY SOURCES

1	www.geerassociation.org Internet Source	1%
2	www.issmge.org Internet Source	1%
3	link.springer.com Internet Source	<1%
4	Steven F. Bartlett, T. Leslie Youd. "Empirical Prediction of Liquefaction-Induced Lateral Spread", Journal of Geotechnical Engineering, 1995 Publication	<1%
5	vdocuments.site Internet Source	<1%
6	www.jiban.or.jp Internet Source	<1%
7	Submarine Mass Movements and Their Consequences, 2007. Publication	<1%
8	assets.researchsquare.com Internet Source	<1%

9	fl-nzgs-media.s3.amazonaws.com Internet Source	<1 %
10	ascelibrary.org Internet Source	<1 %
11	geoenvironmental-disasters.springeropen.com Internet Source	<1 %
12	Jian Zhang, Changwei Yang, John X. Zhao, Graeme H. McVerry. "Empirical models for predicting lateral spreading considering the effect of regional seismicity", Earthquake Engineering and Engineering Vibration, 2012 Publication	<1 %
13	Sharma, . "Mass Movement", Introduction to Process Geomorphology, 2010. Publication	<1 %
14	Daniel T. Gillins, Steven F. Bartlett. "Multilinear Regression Equations for Predicting Lateral Spread Displacement from Soil Type and Cone Penetration Test Data", Journal of Geotechnical and Geoenvironmental Engineering, 2014 Publication	<1 %
15	Encyclopedia of Earthquake Engineering, 2015. Publication	<1 %

16 Kokusho, Takaji. "Major advances in liquefaction research by laboratory tests compared with in situ behavior", Soil Dynamics and Earthquake Engineering, 2016.
Publication

<1%

Exclude quotes	On	Exclude matches	< 5 words
Exclude bibliography	On		